Nanoscale

RSC Publishing

FEATURE ARTICLE

View Article Online
View Journal | View Issue

Bio-inspired magnetic swimming microrobots for biomedical applications

Cite this: *Nanoscale*, 2013, **5**, 1259

Kathrin E. Peyer,[a] Li Zhang[b] and Bradley J. Nelson*[a]

Microrobots have been proposed for future biomedical applications in which they are able to navigate in viscous fluidic environments. Nature has inspired numerous microrobotic locomotion designs, which are suitable for propulsion generation at low Reynolds numbers. This article reviews the various swimming methods with particular focus on helical propulsion inspired by *E. coli* bacteria. There are various magnetic actuation methods for biomimetic and non-biomimetic microrobots, such as rotating fields, oscillating fields, or field gradients. They can be categorized into force-driven or torque-driven actuation methods. Both approaches are reviewed and a previous publication has shown that torque-driven actuation scales better to the micro- and nano-scale than force-driven actuation. Finally, the implementation of swarm or multi-agent control is discussed. The use of multiple microrobots may be beneficial for *in vivo* as well as *in vitro* applications. Thus, the frequency-dependent behavior of helical microrobots is discussed and preliminary experimental results are presented showing the decoupling of an individual agent within a group of three microrobots.

Received 1st September 2012
Accepted 25th October 2012

DOI: 10.1039/c2nr32554c

www.rsc.org/nanoscale

Introduction

Nature has always been an inspiration for robot locomotion, from swimming and wiggling motions, to walking or flying.[1] One of the main challenges for engineering locomotion methods for robots is to copy or mimic the essential functions of their natural counterpart while keeping the complexity low in order to be able to build the system. Building complex devices becomes increasingly difficult in the micro- and nano-scale because the integration of various parts is more challenging. It is, therefore, crucial to capture the essential functionalities of nature while keeping the complexity minimal. Microrobots have

[a]*Institute of Robotics and Intelligent Systems, ETH Zurich, Switzerland*
[b]*Department of Mechanical and Automation Engineering, The Chinese University of Hong Kong, Shatin NT, Hong Kong SAR, China*

Kathrin E. Peyer received her B.Sc. and M.Sc. degree in mechanical engineering at the Swiss Federal Institute of Technology (ETH Zurich) in 2009. She joined the Institute of Robotics and Intelligent Systems lab at ETH Zurich in 2009 as a Ph.D. student. Her fields of interest are bio-inspired robots and swimming microrobots for biomedical applications.

Li Zhang received the Ph.D. degree in physics from the University of Basel, Switzerland, in 2007. From 2002 to 2006, he was also with the Laboratory for Micro- and Nanotechnology, Paul Scherrer Institute, Switzerland. He joined the Institute of Robotics and Intelligent Systems (IRIS), Swiss Federal Institute of Technology (ETH) Zurich, Switzerland, as a postdoctoral fellow in 2007, and as a senior scientist from 2009 to 2012. He is currently an Assistant Professor in the Department of Mechanical and Automation Engineering and an associate faculty member in the Biomedical Engineering Programme at The Chinese University of Hong Kong. His main research interests include design and fabrication of micro-/nano-devices and their biomedical applications, microfluidics, and nanomaterials for energy storage and environmental applications.

been proposed for the use in biomedical applications such as minimally invasive procedures, targeted drug delivery, or *in vitro* for cell manipulation and characterization.[2,3] Most of these applications place these micro-devices into a fluidic or soft environment where they have to be propelled. It is therefore only natural to investigate the locomotion methods found at the microscale in nature for inspiration when building these microrobots.

This article reviews magnetically actuated microrobots for biomedical applications with special focus on bio-inspired systems, in particular the artificial bacterial flagella (ABFs), a swimming microrobot mimicking the helical propulsion of *E. coli* bacteria. ABFs copy the helical shape of *E. coli* flagella, which is the fundamental feature to create forward propulsion, whilst removing the need for a complex on-board rotary motor of *E. coli* by using low-strength rotating magnetic fields for actuation. This article is organized as follows: first, a brief introduction to fluid mechanics at the micro-scale is presented together with an overview of propulsion mechanisms found in nature. Second, the magnetic actuation of microrobots is discussed. Magnetic actuation for microrobots can be separated into two categories, namely force- or gradient-driven microrobots and torque-driven microrobots. A critical comparison of magnetically actuated robots was done by Abbott *et al.* in 2009 and a brief review will be presented.[4] A previous publication by Fischer and Ghosh has already reviewed numerous torque-driven micro- and nanorobotic systems.[5] In the current article a more detailed discussion of other types of magnetic actuation methods is included. Thirdly, the challenges of fabricating 3D helical structures at the microscale are discussed, including a summary of fabrication methods that have been employed successfully to create helical microrobots. Lastly, the use of microrobots in biomedical applications is examined. Potential applications are discussed with emphasis on the use of multiple microrobots. The methods to steer and control individual group members in a larger swarm of microrobots are reviewed and theoretical as well as new preliminary experimental results are presented for individual control of ABFs.

Brad Nelson received mechanical engineering degrees from the University of Illinois (B.S. 1984) and the University of Minnesota (M.S. 1987), and a Ph.D. in Robotics (School of Computer Science) from Carnegie Mellon University (1995). Prof. Nelson has been on the faculty of the University of Minnesota and the University of Illinois at Chicago, has worked at Motorola and Honeywell, and has served as a United States Peace Corps Volunteer in Botswana, Africa. He is the Professor of Robotics and Intelligent Systems at the Swiss Federal Institute of Technology (ETH), Zurich and heads the Institute of Robotics and Intelligent Systems (IRIS).

Micro-scale locomotion in fluids

It is important to consider the Reynolds (Re) number when studying propulsion mechanisms in fluidic environments. The Re number is defined as

$$\mathrm{Re} = \frac{UL\rho}{\eta}, \tag{1}$$

where U and L are the velocity and characteristic length, respectively, and ρ and η are the density and viscosity, respectively, of the fluid. The Re number is a measure of the ratio of inertial to viscous forces in a fluid. For small Re numbers, *i.e.* $\mathrm{Re} \ll 1$, inertial forces become negligible and viscous forces dominate. At the microscale, both U and L are small, and even in water, which is not viewed as a viscous fluid itself, the Re number is much smaller than 1. To understand how micro-organisms move in water, we would have to imagine ourselves swimming in a pool of honey or tar. It then becomes intuitively obvious that the swimming techniques have to be adapted in order to be able to move in such a viscous environment.

Without inertial terms, the flow can be described by the Stokes equations

$$\nabla p = \eta \nabla^2 \boldsymbol{U} + \boldsymbol{f}, \tag{2}$$

where p is the pressure, $\boldsymbol{U}$ the velocity field of the fluid and $\boldsymbol{f}$ external forces on the fluid. This equation is only exact for $\mathrm{Re} = 0$, but it is considered a valid approximation for $\mathrm{Re} \ll 1$. Eqn (2) does not contain any inertial terms and the flow becomes perfectly reversible. As it is a linear equation, the superposition of fundamental solutions is possible. A direct outcome from the reversibility of the Stokes flow is the fact that a perfectly reciprocal motion does not create a net motion. For example, at high Re numbers an oar that is moved up and down at different speeds creates a net propulsive force. At low Re numbers, on the other hand, it is only the geometric configurations that matter, not the speed, and a reciprocal motion leads to no net displacement. This is commonly referred to as the *scallop theorem*.[6] Again it shall be noted that is only true for $\mathrm{Re} = 0$ and in a fluid with constant viscosity. Depending on the size and velocity of the micro-swimmer, small inertial effects still occur that can break the symmetry of the flow. Furthermore, it was shown that the *scallop theorem* breaks down in visco-elastic fluids or even when multiple scallop-type swimmers move as a group.[7,8]

A brief history on microscale propulsion

The propulsion mechanisms of micro-organisms have been the interest of biologists for many years. According to Metzner, as early as the 18th century the flagella of the *Volvox* were already recognized as a propulsion mechanism, but only at the end of the 19th century was it established that all actively propelling micro-organisms have flagella or cilia as means for motion generation. The invention of dark field microscopy allowed the more systematic observation of flagella and cilia in the early 20th century and Metzner presented an overview of detected flagella motions in 1923.[9] Even though the shapes could be observed, their method of generation remained a topic of research for

decades, in particular the motion of helical flagella. An obvious way to generate helical propulsion would be to rotate a rigid helix with a rotary motor. It was, however, assumed that this type of mechanism did not exist as it was not observed anywhere else in nature. In 1966 Doetsch entertained the idea that a rigid helix could be rotated through a basal motor but abandoned this notion only three years later.[10,11] In 1971, in a paper modeling helical propulsion, the author still claimed that rotating joints do not exist in nature,[12] though only two years later, in 1973, Berg was able to prove that *E. coli* bacteria use molecular motors to rotate their helical flagella.[11]

Helical flagella are not the only means of motion generation of microswimmers. A different type of propeller is the flexible flagellum beating in a planar waveform, as for example, in the case of spermatozoa. Another common method is to use cilia, which are generally shorter, hair-like structures covering the outside of the cell body, for propulsion. The mechanism for motion generation for all of these slender tails is based on the drag imbalance on a cylindrical element in combination with a non-reciprocal motion. In the low Re number regime, the drag on a slender cylinder for motion perpendicular to its axis is approximately twice the drag when moving along its axis. When a slender cylinder is pulled at an oblique angle it moves with an angle of attack due to the drag imbalance. This results in a velocity vector that has components in the pulling direction as well as perpendicular to it. This is taken advantage of when flagella or cilia are employed for motion generation.

As mentioned previously, the filament has to be moved in a set of non-reciprocal configurations in order to generate a net motion. In the example of cilia, they are stretched out during the power stroke and glide close by the body in recovery stroke. In the case of a flagellum beating in a planar wave pattern each segment of the flagellum goes through a non-reciprocal motion as it moves from a positive angle of attack to moving with a negative angle of attack *versus* the swimming direction. A segment on a rigid helix always has the same angle of attack to the direction of motion and each segment goes through a non-reciprocal motion only while the helix is continuously rotated. If a helix is rotated by a positive angle and then rotated back by the same angle, the motion becomes reversible and the helix moves back into its original position.

Bio-inspired microrobots and micro devices

The various propulsion mechanisms of micro-organisms have in turn inspired a number of magnetic microrobot designs (see Fig. 1). A flexible flagellum is arguably the easiest mechanism to copy as it is a one dimensional (1D) structure. A challenge that remains is to fabricate a simultaneously flexible and stable structure at the microscale. A flexible sheet or beam can be actuated magnetically when attached to a magnetic head.[13,14] Dreyfus *et al.* presented another approach to form a flexible flagellum. They used self-assembled magnetic beads to form a flexible tail (see Fig. 2a).[15] The magnetic force between magnetic beads is limited and fast rotation of these bead chains can lead to a disassembly due to the fluidic drag forces.[16] Hence, Dreyfus found a protocol to connect the magnetic particles with DNA strands. It was shown that a chain of beads actuated with an oscillating field does not result in a non-reciprocal motion; however, attaching a payload to one end of the chain breaks the motion symmetry of the traveling wave along the bead chain. In this way, the transport of a single red blood cell (RBC) was demonstrated. It was shown that a kink in the chain also breaks the symmetry and allows propulsion.[17,18] The fact that an imperfect or asymmetric chain can achieve propulsion was utilized for the nano-bead chain swimmer presented by Benkoski.[19,20] The length of some of their swimmers is only around 5 μm, which is smaller than Dreyfus' propeller, which had an overall length of approximately 24 μm, by a factor of almost five.

The first helical microrobot mimicking bacterial propulsion, the artificial bacterial flagellum (ABF), was presented in 2007 by Bell and further characterized by Zhang in 2009.[21–23] The ABF consists of a rigid helical tail which is attached to a soft-magnetic metal "head", also referred to as "body", for actuation (see Fig. 2b). The size of the helical tail is 2.8 μm in diameter and 30–100 μm in length. The head consists of a thin square plate, with a thickness of 200 nm and a variable length of 2.5–4.5 μm. The main challenge for bacteria-inspired microrobots is the fabrication of a helical filament at the microscale. In recent years, a number of fabrication methods have been found that are capable of small-scale helix fabrication. They will be discussed in more detail in the section "Fabrication of helical

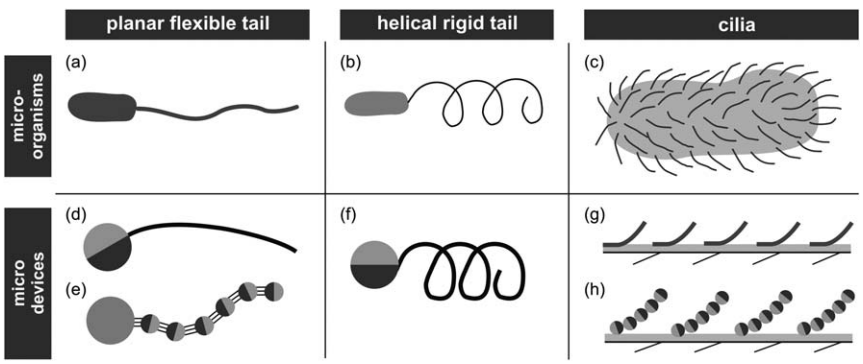

Fig. 1 Propulsion mechanisms of microorganisms and analogous artificial propulsion of magnetic micro-devices. (a) Planar beating of flexible flagella, *e.g.* spermatozoa. (b) Rotating rigid helical flagella actuated by a molecular motor, *e.g. E. coli* bacteria. (c) Cilia, *e.g.* paramecium. (d) Flexible beam actuated by a torque at the spherical head. (e) Flexible magnetic micro-bead tail. (f) Rotating rigid helical tail fixed to a magnetic head. (g) Artificial cilia array of flexible micro rods or beams. (h) Artificial cilia array of self-assembled magnetic micro-beads.

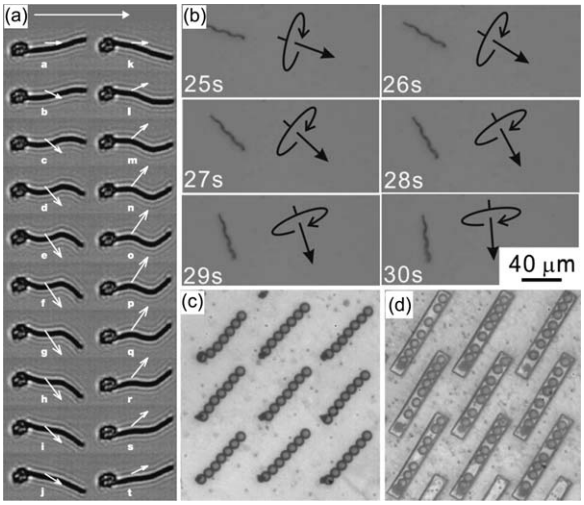

Fig. 2 Biomimetic magnetic micro-devices. (a) Flexible tail of micro-beads attached to a blood cell.[15] (b) Steering of a helical microrobot.[22] (c) Superparamagnetic bead cilia assembled by optical tweezers and (d) self-assembled.[33] Reused with permission.[15,22,33]

micro-structures". What they all have in common is that the helical tail is a rigid structure, but the application of a magnetic material is not always restricted to the head, but may be directly applied to the tail as well.[24,25]

Cilia were one of the earliest intensively studied filaments in nature.[26] They are not only a means to propel micro-organisms, such as the famous paramecium, but they also function as stationary fluid transporter, for example, to move mucus in our airways.[27] Cilia usually cover the whole surface and move in coordination with each other, similar to a traveling wave seen in the feet motion of centipedes. If cilia motion was to be mimicked in this way, an independent actuation for each cilium would be required. This behavior has been studied and reproduced experimentally using microtubules.[28] Artificial magnetic cilia, by contrast, move simultaneously. There are to this day no motile microrobots that use cilia for propulsion. Instead, artificial cilia are used on surfaces to transport fluids, for example, in lab-on-a-chip applications, such as the pumping and mixing of micro-fluids. The two main approaches for fabricating artificial cilia are etching of slender beams or rods using lithography[29–34] or using self-assembled magnetic beads (see Fig. 2c and d).[35–38]

Modeling helical propulsion

There have been numerous papers published on the modeling of micro-organisms using planar or helical tails for propulsion. Many of the fundamental solutions for slender flagellum propulsion were published before the discovery of the rotary motor of *E. coli* bacteria.[39–41] Helical propulsion has since become a growing area of interest for both biologists and engineers.[4,42–47] A very intuitive approach for modeling slender body dynamics at low Re numbers is the resistive force theory (RFT). RFT assigns a local drag coefficient to a segment, *i.e.* cylindrical element, of a slender filament. The resistive force coefficients (RFC) are derived based on the slender body theory, which approximates a slender filament by a line distribution of singularity solutions, and various coefficients have been suggested and evaluated.[42,43,48] The drag on this cylindrical element is anisotropic with the drag perpendicular to the cylindrical axis being larger than the drag parallel to the axis by an approximate factor of two. The factor two is a theoretical maximum and is smaller for real filaments, *i.e.* for a filament with a finite slenderness. Lighthill's RFCs for an infinitesimal cylindrical element on a helical tail are[42]

$$\xi_{ll} = \frac{2\pi\eta}{\ln(2q/r) - 0.5},\ \xi_n = \frac{4\pi\eta}{\ln(2q/r) + 0.5} \tag{3}$$

where ξ_{ll} and ξ_n are the drag coefficients along and perpendicular to the cylindrical axis, respectively; r is the radius of the filament and $q = 0.09\lambda$, where λ corresponds to the pitch of the helix. These coefficients are given per unit length and the force on an infinitesimally small filament of length ds is

$$\mathrm{d}f_{ll} = u_{ll}\xi_{ll}\mathrm{d}s,\ \mathrm{d}f_n = u_n\xi_n\mathrm{d}s \tag{4}$$

where ds is an infinitesimal line segment along the helix. The local filament velocities u_{ll} and u_n are given by a transformation of the body velocity into the local filament coordinate system. To get the total drag forces on the helical tail, the local filament forces df_{ll} and df_n can be transformed into the body coordinate system and integrated along the whole length of the helix (see Fig. 3).

For steady-state motion, the externally applied forces and torques have to equal the drag on the swimmer. Purcell presented a simplified 1D model, where helical motion is described only by the rotation and translation along the helical axis.[6] The result is a 2 × 2 propulsion matrix relating the velocity and rotational speed to the external force and torque:

$$\begin{bmatrix} F \\ T \end{bmatrix} = \begin{bmatrix} a & b \\ b & c \end{bmatrix} \begin{bmatrix} u \\ \omega \end{bmatrix} \tag{5}$$

The coefficients a, b, and c are functions of geometric parameters and fluid viscosity only. They can be modeled with RFT, resulting in[4]

$$a = 2\pi nR\left(\frac{\xi_{ll}\cos^2(\alpha) + \xi_n\sin^2(\alpha)}{\sin(\alpha)}\right) \tag{6}$$

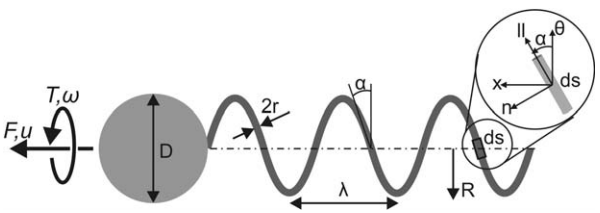

Fig. 3 1D model of the helical microswimmer. F and u are the force and velocity along the helical axis, respectively. T and ω are the torque and rotational speed around the helical axis. The geometric model parameters of the tail are the helix radius R, pitch λ, helicity angle α and filament thickness r. The head is modeled by a sphere with diameter D. Inset shows the local coordinate system of the infinitesimal segment ds.

$$b = 2\pi n R^2(\xi_{\parallel} - \xi_{\perp})\cos(\alpha) \quad (7)$$

$$c = 2\pi n R^3\left(\frac{\xi_{\parallel}\sin^2(\alpha) + \xi_{\perp}\cos^2(\alpha)}{\sin(\alpha)}\right) \quad (8)$$

R is the radius and α is the helicity angle of the helix. Eqn (6)–(8) are valid for helices with an integer n number of turns. From the propulsion matrix of the helical tail (5) it can be seen that the rotary and translational motions are coupled by the off-diagonal elements b. Hence, an externally applied force can induce a rotary motion or, *vice versa*, a torque can induce a translational motion. The head or body of a helical micro-swimmer can be approximated by a sphere, which has a translational drag ψ_v and rotational drag ψ_ω of

$$\Psi_v = 3D\pi\eta,\ \Psi_\omega = D^3\pi\eta \quad (9)$$

As a propulsion matrix, this can be written as:

$$\begin{bmatrix} F \\ T \end{bmatrix} = \begin{bmatrix} \Psi_v & 0 \\ 0 & \Psi_\omega \end{bmatrix}\begin{bmatrix} u \\ \omega \end{bmatrix} \quad (10)$$

The drag on a sphere is isotropic and no coupling between the rotational and translational motion exist. Hence, the off-diagonal elements are equal to zero. Under the assumption that the flow of the head and tail do not influence each other, the propulsion matrix of the entire swimmer can be calculated by summing up the matrix elements of the tail and head:

$$\begin{bmatrix} F \\ T \end{bmatrix} = \begin{bmatrix} a + \Psi_v & b \\ b & c + \Psi_\omega \end{bmatrix}\begin{bmatrix} u \\ \omega \end{bmatrix} \quad (11)$$

When considering the motion along the helical axis, the 1D propulsion matrix is often a sufficient means to model the behavior of a helical micro-swimmer. For more complex problems, for example, when modeling off-axis forces or motion, the propulsion matrix needs to be established in 3D. The result is a 6×6 matrix, with A, B and C being 3×3 matrices, of the form:

$$\begin{bmatrix} F \\ T \end{bmatrix} = \begin{bmatrix} A & B \\ B & C \end{bmatrix}\begin{bmatrix} U \\ \Omega \end{bmatrix} \quad (12)$$

The entries of A, B and C were modeled analytically using RFT for the implementation of a gravity compensation algorithm or for modeling the near-boundary motion of bacteria.[49,50] For the considerations in this article the 1D model from eqn (11) will be sufficient.

Actuation methods for swimming microrobots

In our review, we use the term "swimmer" broadly to refer to all types of microrobots moving or being moved in a fluidic environment. Just like their natural counterparts, microrobots function only in a suitable environment that provides nutrition or energy supply, respectively. Even though bacteria-inspired robots have been built with onboard motors and tethered to an external power source,[47] this approach is not feasible when the size of the device reaches the micro-scale. The main challenge lies, therefore, in providing an environment for microrobots that

(a) enables them to harvest energy for their locomotion, and
(b) conforms to the application environment requirements.

It transpires that solving (a) is somewhat easier to achieve, and there have been numerous successful approaches presented in the literature in recent years. One idea is to use natural swimmers as a propulsion mechanism. Single paramecia[51] or swarms of flagellated bacteria have been steered successfully and employed for the transportation and manipulation of micro-objects.[52–56] Their advantage is obvious – they can gather nutrition directly from their environment and turn it into energy for their propulsion system, which has already been optimized through an evolutionary process. Unfortunately, their disadvantage is caused directly by their advantage, namely that the micro-organisms have to be kept in an environment that contains nutrition and has suitable chemical conditions. Furthermore, the microorganisms live comfortably only in a certain temperature range that may not conform to the temperatures encountered in the application. For example, when MC-1 bacteria were tested in temperatures of 37 °C, which is an essential requirement for the application in the human body, the propulsion speed decreased with time and reached almost zero after 40 minutes of experimentation.[55]

Using artificial devices removes the need for a nutritious environment and they can potentially function under various temperature conditions. In recent years, numerous prototypes of micro- and nanobots have been proposed that use electrochemical decomposition to propel themselves.[57] Devices relying on chemical fuel use a similar approach to bacteria by harvesting chemical compounds for propulsion generation directly from their environment. Most commonly, the electrochemical reaction uses hydrogen peroxide, which is added to the microbots' environments. These catalytic microbots were employed successfully *in vitro* for cell transportation tests.[58] It may, however, be difficult to apply these results *in vivo* as the creation of the required chemical environment inside the human body remains a challenge.

Using magnetic fields for the actuation of microrobots supports various propulsion methods of micro-devices and also fulfills the requirement (b) very well. Low-strength and low-frequency magnetic fields are considered harmless to living organisms including the human body. Furthermore, magnetic fields can travel through water undisturbed, which allows them to penetrate through the human body unabsorbed. In this way, a magnetic environment for the microrobots to propel themselves can be applied remotely. This approach is suitable for *in vitro* as well as *in vivo* applications.[2,3] The use of magnetic fields for actuating microrobots is, however, not without its challenges. An electromagnet or a strong permanent magnet can be used as a source for supplying the magnetic environment to the microrobot but the magnetic field decays rapidly with the distance from the source. This has to be accounted for when designing magnetic actuation setups and choosing magnetic propulsion methods (see section "How should microrobots swim?" for more details).

Magnetic actuation principles

The basic principle of magnetic actuation is to apply a magnetic force or a torque on a magnetized micro- or nano-object. A magnetized object in a magnetic field experiences a torque $\boldsymbol{T}_m$ [N.m] that acts to align its magnetization $\boldsymbol{M}$ [A.m^{-1}] with the external field $\boldsymbol{B}$ [T].

$$\boldsymbol{T}_m = V\boldsymbol{M} \times \boldsymbol{B} \tag{13}$$

V [m^3] is the volume of the magnetic object. The magnetic force $\boldsymbol{F}_m$ [N] on an object with volume V is given by

$$\boldsymbol{F}_m = V(\boldsymbol{M}\nabla)\boldsymbol{B} \tag{14}$$

The object can be permanently magnetized or it can be soft-magnetic, paramagnetic or superparamagnetic and become magnetized only while under the influence of the externally applied magnetic field. Hence, $\boldsymbol{M}$ can be constant in the case of a hard magnet or is a function of the applied field and the geometry of the object.

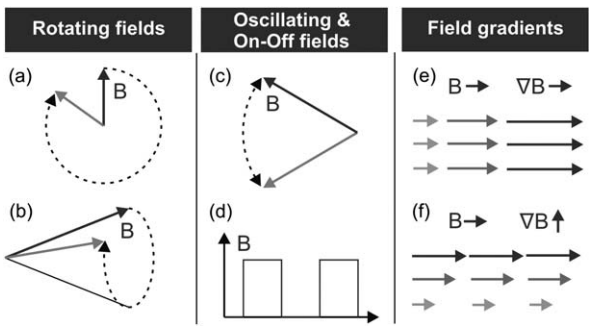

Fig. 4 Magnetic actuation methods. (a) Field vector rotated in a plane. (b) Field rotated along the mantel of a cone (precession field). (c) Oscillating "up–down" field in a plane. (d) On–off field. (e and f) Magnetic field gradients; (e) field gradient along the direction of the field and (f) field gradient perpendicular to the direction of the field.

A microrobot in a uniform magnetic field does not experience any force, only a torque, until $\boldsymbol{M}$ is collinear with $\boldsymbol{B}$. At this point the torque $\boldsymbol{T}_m$ becomes zero and the microrobot remains immobile. In order to generate a continuous actuation, the magnetic field has to (a) go through a spatial change, *i.e.* exhibit a field gradient, or (b) go through temporal change, such as a rotation, precession, oscillation or on–off states (see Fig. 4). The first version (a) produces a magnetic force with which microrobots can be pulled, removing the need for an additional swim mechanism. Version (b) allows the design of a number of robot types with various actuation principles (see Fig. 5).

Rotating fields are characterized by the field vector going through a complete and continuous rotation around an axis. Generally, the field vector rotates in a plane perpendicular to the rotation axis. For a precession-type field, on the other hand, the vector forms the mantle of a cone. Helical microrobots are actuated by rotating magnetic fields. The swimmer is rotated around its helical axis and the direction of motion is perpendicular to the plane of rotation.[22] Flexible nanorods can also be actuated by a rotating field, although better results were reported by using a precession-type actuation. They consist of two parts, gold and nickel, connected by a thinly etched silver connector that is flexible. Depending on the relative size of the two end-parts, the resulting translation is in the positive or negative direction along the axis of rotation.[59]

Rotating fields can also be employed for the actuation of "surface walkers". The term is used in literature for some of the devices, and refers to the fact that this propulsion mechanism is based on the proximity of the robot to a surface. It may be somewhat misleading because the propulsion mechanism can also work without direct contact. The propulsion is induced either by a rolling or tumbling along the surface with contact, or by a contact free "rolling" with slip. Due to the presence of a wall the apparent viscosity increases towards the surface and this drag imbalance causes the microrobots to "roll" or tumble along the surface. Unlike the helical propeller, this type of

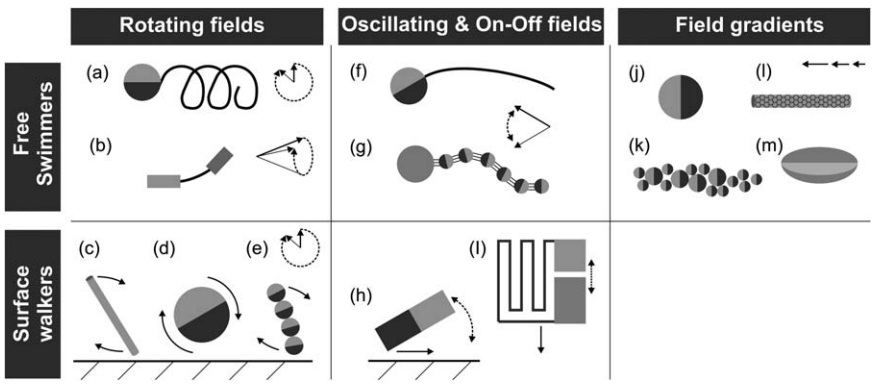

Fig. 5 Types of magnetic microrobots and their actuation methods. One can distinguish between free-swimming microrobots, or robots that propel only due to a nearby boundary (surface walkers). (a) Helical microrobot actuated by a rotating field. (b) Flexible nanorod actuated by a rotating or precession field. (c)–(e) Actuated with a rotating field, these microrobots tumble along the surface due to the fluidic drag imbalance. In this schematic, they would all tumble from left to right along the surface. (c) Nanorod; (d) permanent magnetic sphere; (e) self-assembled micro-bead chains. (f and g) In-plane oscillating fields actuate the head and tail respectively. (h) Due to surface friction, this robot etches forward with every up-down oscillation. (l) Top view of a wireless resonant actuator, powered by on–off field oscillations. (j)–(m) Different types of nano- and microrobots pulled by field-gradient forces. (j) Single permanent magnet; (k) multiple magnetic beads that group to attractive forces between them; (l) nickel or iron-filled carbon nanotubes and (m) soft-magnetic assembled microrobot.

motion occurs in the same plane as the rotating magnetic field. The simplest example is the rolling of a permanently magnetized sphere.[60,61] Similarly to the artificial cilia mentioned previously, self-assembled chains of magnetic micro-beads can be used to tumble along surfaces (see Fig. 6a).[62–64] With the help of gravity or magnetic forces, almost arbitrarily shaped microrobots can be propelled along surfaces.[64–66] Nickel nanowires can be propelled by the fluidic drag imbalance without direct contact with the surface. In this manner, they were propelled not only along a flat surface, but also up along vertical walls against gravitational forces. Furthermore, they were employed for cargo transport either by attaching the cargo to the wire or by using local microvortices created by the rotating wire.[67–69] An interesting type of surface propulsion was reported recently using self-scrolled tubular helices. These hollow-bar-, corkscrew- and radial-magnetized helices tumble, wobble or roll along surfaces under the application of a rotating magnetic field.[70,71]

Oscillating and on–off fields summarize all temporal magnetic fields apart from the rotating fields. The most common type of oscillation is characterized by a field vector moving up and down in the plane. In this manner flexible-flagella-type swimmers can be actuated.[14,15] Another way to use oscillating fields is for surface propulsion with a slip–stick type motion. A magnetic micro-bar, or Mag-μBot, is rotated upwards quickly, resulting in a slight forward sliding motion (see Fig. 6b). Then the field is rotated downwards and the magnetic micro-bar rotates around its corner that is in contact with the surface.[72,73] Another type of temporally changing fields is the on–off actuation employed by MagMites or PolyMites.[74–76] MagMites and PolyMites are wireless resonant magnetic micro-actuators. They consist of a spring connecting two asymmetric soft-magnetic bodies. When the magnetic field is switched on, the bodies magnetize and attract each other, which results in an elongation of the spring (see Fig. 6c). Then the field is switched off and the restoring spring energy moves the bodies apart. This on–off cycle occurs in the range of kHz, corresponding to the Eigen frequency of the system. In this way, the resonant mode can be used, thereby increasing the amplitude of the oscillating motion, and even a collision of the magnetic bodies can be achieved. This impulse enhances the forward edging that occurs with each cycle.[77]

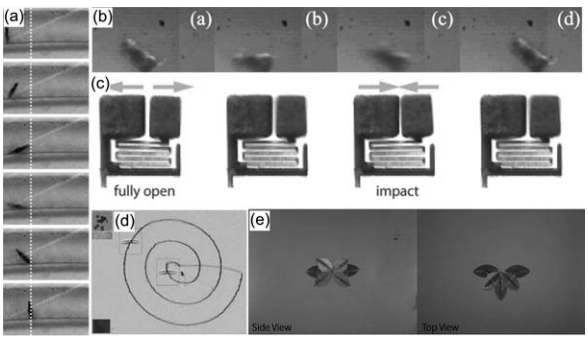

Fig. 6 (a) Self-assembled microbeads surface walker.[64] (b) Slip–stick motion of an oscillating Mag-μBot.[104] (c) Top view of a MagMite during one cycle of oscillation.[75] (d) Trajectory-following nanowire actuated by magnetic field gradients.[80] (e) Soft-magnetic assembled microrobot. Overlay image of the trajectory from the top and side view.[84] Reused with permission.[64,75,80,84,104]

Field gradients are used to exert forces on the microrobots. Microrobots are always attracted towards the strongest field, *i.e.* along the positive field gradient. The robot aligns itself with the direction of the field, as given by eqn (13), and moves in the direction of the field gradient, which does not have to coincide with the orientation of the field. Magnetic micro- and nanorobots of any kind can be moved with gradient forces. The most common shapes are spherical[78,79] or rod-shape microrobots, such as nanowires (see Fig. 6d).[80] The elliptical body is close to the minimum drag shape at low Re numbers[81,82] and was investigated for the use in eye-surgery (see Fig. 6e).[83–85] Magnetized robots themselves turn into tiny local dipoles that attract each other. Hence, groups of spheres, micro- or nanoparticles, or nanowires agglomerate and can be actuated as a whole.[86]

Magnetic setups

The magnetic field of a single source, such as a permanent magnet or electromagnetic coil, can be approximated by a dipole model (see also section "How should microrobots swim?"). A magnetic field and a field gradient are created at the same time but they are inherently coupled. In order to set the field strength and field gradient independently (along a single axis), at least two sources are required. The design problem is similar to building a robotic arm manipulator and providing the correct number of actuators for the desired degree of freedom (DOF). For example, if a robot arm is to reach all points in 3D (three DOFs), with arbitrary orientation at the tip (another three DOFs), at least six actuators are required. Using six actuators, however, does not guarantee six DOFs of the manipulator in the whole workspace as there can be singularities in certain configurations. One way to solve this problem is to use a redundant robot arm, *i.e.* a robot arm with more degrees of actuation than degrees of freedom. Similar results were shown for the magnetic gradient actuation of microrobots. For moving microrobots with five or six DOFs, an 8-coil setup was constructed. This removed the occurrence of singularity configuration in the workspace and minimized the actuation power of the whole system. Intuitively, a magnetic force appears to be a straightforward approach for moving microrobots but it is in fact a complex control problem as it is inherently an unstable system.

An alternative approach for generating magnetic fields is to use a permanent magnet. As presented in the previous section, in order to control microrobots the magnetic field has to be varied – either spatially or temporally. With electromagnetic coils the magnetic field is varied by adjusting the current and the setup itself remains stationary. By contrast, a permanent magnet creates a fixed-strength magnetic field. In order to vary the field, the magnet itself has to be moved in space closer to or further away from the microrobot. This can be achieved by attaching the magnet to a robotic arm. Furthermore, the magnet can be attached to a rotary motor to achieve rotating magnetic fields.[87] The successful control of helical (screw-type) as well as spherical microrobots was demonstrated by Mahoney *et al.*[61,88,89]

How should microrobots swim?

As shown in the previous section, magnetic fields can be used to power numerous types of microrobots. Naturally, the question arises which mechanism is best suited to power magnetic microrobots. A comparison of all the various microrobot designs is beyond the scope of this article, but Abbott *et al.*[4] formulated some fundamental considerations, which shall be discussed in this section.

Torque-driven *versus* force-driven magnetic microrobots

Many bio-inspired robots use a type of tail for the propulsion generation. Commonly, they are torque-driven microrobots, either using a rigid helical tail, or a flexible tail that is deflected due to the fluidic drag encountered. Purcell calculated the efficiency of propulsion by taking the power for simply pulling a sphere in a fluid over the power used for propulsion (see Fig. 7).

$$\varepsilon = \frac{Fv}{T\omega} \tag{15}$$

With this definition, a helically propelled sphere has an efficiency value in the order of 1%. The reason lies in the fact that a helix moving through fluid does not advance by one pitch per rotation. Instead, it slips by a large amount, moving only by a small percentage of its pitch. The efficiency of a flexible tail is the same order of magnitude. A microrobot actuated by a gradient-force, on the other hand, has always an efficiency of 100% according to eqn (15). This measure can be somewhat misleading, as it does not account for how the power from a magnetic actuation setup is transferred to the robot.

Abbott proposed to compare the force- and torque-driven robots by assuming an equal input to a magnetic coil setup consisting of a pair of identical coils with radius b placed at a distance of $2L$ to each other. The field in the centre is the summation of the fields created by the two coils. For a torque-driven microrobot, no gradient force is necessary, only a field is required. Running a current i through the coils in the same direction, creates the maximal field, while producing a zero field gradient. If the current is run in opposite directions, the field is zero, but the maximal field-gradient is achieved. In this manner, torque-driven and force-driven microrobots can be directly compared, as their power is provided by identical coils with an identical input, *i.e.* the current i. The field and gradient in the centre of the coils are given by[4]

$$|\boldsymbol{B}| = \frac{b^2}{(b^2+L^2)^{3/2}}\mu_0 i \tag{16}$$

and

$$\nabla|\boldsymbol{B}| = 0 \tag{17}$$

for the current i running in the same direction, respectively, and

$$|\boldsymbol{B}| = 0 \tag{18}$$

and

$$\nabla|\boldsymbol{B}| = \frac{3b^2L}{(b^2+L^2)^{5/2}}\mu_0 i \tag{19}$$

for the current i running in opposite directions (see Fig. 8). Combining the magnetic actuation with the fluid mechanical models in eqn (10) and (11) allows the direct comparison of the maximum velocity and propulsive force of a sphere being

(a) pulled by a magnetic force, or

(b) rotated by a torque and propelled by a helical tail.

For solving (a), eqn (10), (14) and (19) can be combined and the following simple system of equation has to be solved:

$$\begin{bmatrix} F_{\mathrm{m,max}} \\ 0 \end{bmatrix} = \begin{bmatrix} V|\boldsymbol{M}|\nabla|\boldsymbol{B}| \\ 0 \end{bmatrix} \overset{!}{=} \begin{bmatrix} \Psi_v & 0 \\ 0 & \Psi_\omega \end{bmatrix} \begin{bmatrix} u_{\mathrm{pull,max}} \\ \omega_{\mathrm{pull,max}} \end{bmatrix} \tag{20}$$

Clearly, $\omega_{\mathrm{pull,max}}$ is equal to zero as no torque is applied to the sphere and $u_{\mathrm{pull,max}}$ can be found from the first line of the matrix equation. For solving (b), eqn (9), (13) and (16) can be combined to:

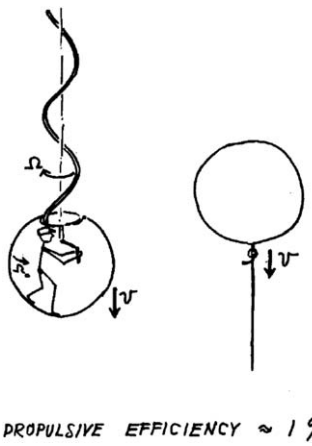

Fig. 7 Sketch by Purcell comparing the propulsion of a spherical body through pulling or helical propulsion. Reused with permission.[6]

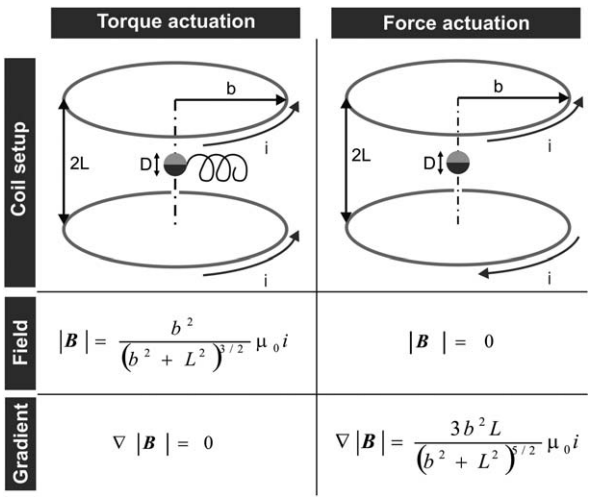

Fig. 8 Coil setup for comparing torque-driven and force-driven magnetic microrobots based on Abbott *et al.*[4]

$$\begin{bmatrix} 0 \\ T_{\mathrm{m,max}} \end{bmatrix} = \begin{bmatrix} 0 \\ V|\boldsymbol{M}||\boldsymbol{B}| \end{bmatrix} \overset{!}{=} \begin{bmatrix} a+\Psi_v & b \\ b & c+\Psi_\omega \end{bmatrix} \begin{bmatrix} u_{\mathrm{helix,max}} \\ \omega_{\mathrm{helix,max}} \end{bmatrix} \quad (21)$$

From eqn (22) $u_{\mathrm{helix,max}}$, which is coupled to $\omega_{\mathrm{helix,max}}$, can be found. The assumptions are that the helical tail has a radius of equal to the sphere radius $R = D/2$. Furthermore it is assumed that the sphere is permanently magnetized, *i.e.* that $\boldsymbol{M}$ has a constant value independent of the applied magnetic field. The magnetic torque and force scale, however, with the volume V, *i.e.* with $\sim D^3$.

The result showed that for a given setup, *i.e.* a given b, L and i, the maximum velocity scales with $\sim D^2$ for a gradient-driven sphere and with $\sim D$ for a torque-driven helically propelled sphere. Similarly, the maximum propulsive force can be shown to scale with $\sim D^3$ for a gradient-driven sphere and $\sim D^2$ for a torque-driven helically propelled sphere. This suggests that, at a sufficiently small value of D, the torque-driven microrobot outperforms the gradient-driven microrobot. Despite the low efficiency of helical propulsion, the torque-driven microrobot can outrun the force-driven microrobot because of how the actuation power can be transferred and utilized. The question at which critical size of D the helical propulsion overtakes gradient-pulling was not directly answered, as it depends on many parameters, including the setup design. For realistic assumptions, *e.g.* a coil distance L such that a robot could be actuated inside a human eye, helical propulsion outperformed gradient-pulling already at the millimeter-scale. The authors acknowledged that the model uses many simplifying assumptions; however, the physics of how these two actuation mechanisms scale is not expected to change fundamentally. Thus, we can expect that torque-driven robots will be able to outperform gradient-driven robots as their size shrinks from the millimeter to the micro- and, further still, the nanometer scale. It is important to keep in mind that this model only considers the magnetic actuation and not, for example, other hardware limitation for generating rotating magnetic fields. In the model described above, it was assumed that the maximum rotation frequency necessary to achieve v_{max}, can be implemented, which may not always be the case. For the complete discussion of magnetic force-driven *versus* torque-driven swimming microrobot, please refer to Abbott *et al.* (2009).[4]

Fabrication of helical micro-structures

Torque-driven free-swimming microrobots either use a rigid helical tail or a flexible tail (see Fig. 5). The advantage of a rigid tail is that propulsion in confined spaces should be possible without changing the actuation input, which might be necessary for a floppy tail (*e.g.* adjusting the wave amplitude). Furthermore, a helix can be propelled forwards or backwards simply by reversing the direction of rotation of the magnetic field. The straightforward maneuvering of torque-driven helical microrobots makes them a promising tool for biomedical applications.[90] One of the main challenges is, however, the fabrication of these complex 3D structures at the micro- and nanometer scale.

Helices can be considered a fundamental shape of nature, and are found at numerous scales even down to the size of our DNA. There are a number of approaches for fabricating micro and even nano-helices, but the main challenges for fabricating microrobots are the repeatability of the process, the control over design parameters and, more specifically, the application of

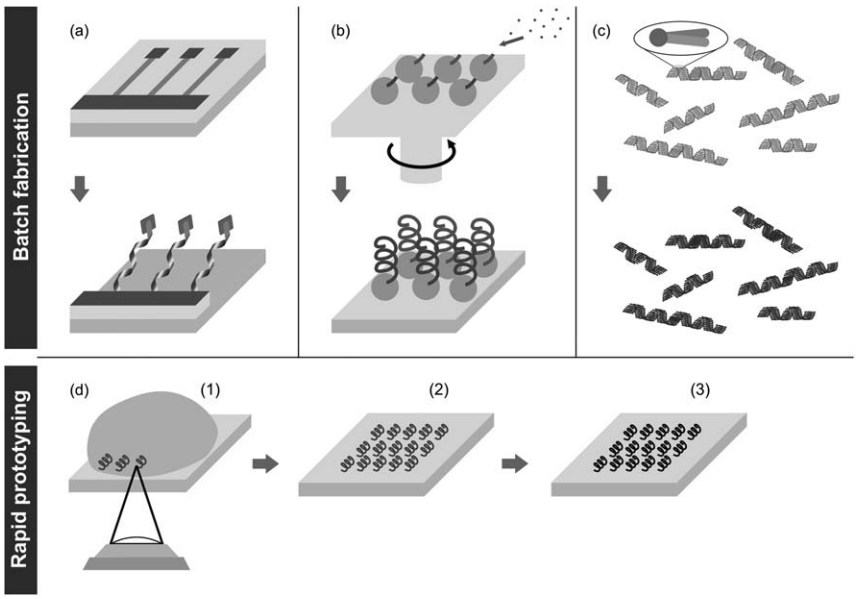

Fig. 9 Fabrication methods. (a) Self-scrolling method for ABF fabrication. Bi- or tri-layered thin-film ribbons and a square nickel head are grown and deposited, respectively. After wet-etching, the ribbons curl into helices in a controlled manner. (b) GLAD fabricated helices. Pillars are deposited at an angle and under constant rotation of the stage, resulting in helices on the spherical seeds. (c) Helical liposome scaffolds self-assembled in a lipid dispersion. After a palladium seeding, a magnetic cobalt alloy was grown *via* electroless deposition. (d) 3D lithography with a direct laser writing tool. (1) Polymerization of the photoresist at the focal point of the laser; (2) development and subsequent rinsing and (3) magnetic metal coating.

magnetic material necessary for the actuation. The first functional helical microrobot, the ABF, was presented by Bell *et al.* in 2007. The fabrication was based on the self-scrolling technique, which relies on the (controlled) internal stress of thin material layers to roll into a desired 3D shape (see Fig. 9a). The crystal orientation defines the rolling direction of the bi- or tri-layer ribbon. Hence, the direction of the ribbon on the substrate defines the helicity angle. The radius of the helix is adjusted by tuning the thickness of the ribbon. This method was known before 2007, but the ABF was the first swimming microrobot design with a nickel head for magnetic actuation. The square width and thickness of the nickel head can be adjusted with the lithography step and metal deposition step, respectively.[22,23]

In 2009, even smaller helices were fabricated by glancing angle deposition (GLAD). This method uses spherical seeds on which helical pillars are grown through the rotation of a tilted stage during evaporation (see Fig. 9b). They were magnetized by depositing a cobalt layer along one half of the helix and permanently magnetizing it perpendicular to the helical axis in a subsequent step.[24] More recently, the fabrication of nano helices was demonstrated through electroless deposition of a cobalt composite on helical lipids (see Fig. 9c). These lipids scroll into helices, and their pitch is tuned by the alcohol concentration. It was shown that a radial magnetization could be achieved that allowed the rotation of the lipids around their helical axis.[91]

The methods mentioned above can be described as batch fabrication processes. The self-scrolling and GLAD methods create very uniform helix designs. The lipids are less uniform, for example, the length of the helices cannot be controlled, and suitable structures have to be found within the solution. There is another approach for controlled fabrication of micro helices, based on 3D lithography, which is not a batch fabrication process (see Fig. 9d). A laser beam is focused into the photoresist and a two-photon polymerization (TPP) occurs at the focal point of the laser. A piezoelectric stage moves the glass substrate with the photoresist in 3D following a pre-programmed trajectory. In this manner, polymer structures of arbitrary shapes can be written. With this "microscale rapid prototyping", various design features can be added to the helical base shape, such as, for example, a claw for micro-object transport.[25] The method is not limited to fabricating only a few microrobots. Arrays of thousands of micro-structures can be fabricated within a few hours. They can be detached manually or *via* sonication to create suspensions of microrobots.[90,92]

The magnetic material can either be deposited in a subsequent step by evaporation[24] or micro particles can be incorporated in the polymer before the laser writing step.[93] This results in soft-magnetic material being deposited along the whole of the helical structure, similarly to the magnetic lipids, and, consequently, the direction of magnetization is not obvious. The optimal magnetization direction for a helical microrobot is perpendicular to the helical axis to maximize the applicable magnetic torque around the axis. The first ABF design relied on the shape features of the head to give a preferred magnetization direction. The GLAD-prototype used a permanently magnetized film in the radial direction. With soft-magnetic material along the whole length of the tail, the magnetization is not yet well understood and little research exists. Tottori *et al.* presented experimental data showing how the magnetization changes with the pitch of the helix but further investigations are necessary.[25] Nevertheless, these types of swimmers can be actuated by a rotating magnetic field as the swimmers align themselves such that they rotate around their helical axis at moderately high frequencies. This frequency-dependent orientation of helical swimmers was reported previously but also requires further investigation.[94]

Towards swarm control in biomedical applications

The potential uses of swimming microrobots can be divided into *in vitro* and *in vivo* application areas. Medical applications in the human body mainly focus on targeted drug delivery. The ablation of the material and the delivery of hyperthermia for cancer treatment have also been discussed but the size of the robots may have to be increased to the millimeter scale for these types of tasks.[2,95] Potential *in vitro* or lab-on-a-chip applications include the manipulation and characterization of cells and micro-fluid control.[3] Artificial bacterial flagella have been employed for flow manipulation for non-contact manipulation of micro-objects as well as for micro-object transportation.[25,96] The performance of a single microrobot agent employed for manipulation or delivery tasks could be improved by using multiple robots, for example, to generate more complex flow fields[97] or to better distribute drug loads, respectively. It is, therefore, foreseen that not only single devices, but whole swarms of microrobots will be employed in various types of biomedical applications. This necessitates the control of groups of microrobots, either as a whole unit, or by addressing individual agents to navigate them independently.

Magnetic actuation naturally lends itself towards the uniform control of microrobot swarms. The reason lies in the fact that all microrobots receive the same magnetic field input. In fact, no more power is required to actuate one microrobot than it is to actuate hundreds of microrobots within the same work space. More challenging is the task to steer individuals or groups of microrobots separately from each other. Separate control of microrobots is usually achieved by employing inhomogeneous robot designs. Microrobots that use the same type of input, *e.g.* rotational or oscillating magnetic fields, can be fabricated with different design parameters. The goal is to achieve a variable velocity at the same input signal. This may entail a variable speed or a different direction of motion. There have only been a few publications that have shown individual control of microrobots. A short review will be given on two types of "surface-walkers", followed by a more detailed discussion of individual control of helical swimming microrobots.

Individual control of surface-walkers

MagMites use an oscillating magnetic field for actuation. The actuation occurs at the Eigen frequency of the mass–spring system. The Eigen frequency of this oscillator can be tuned by

designing the masses and spring stiffness accordingly. It was demonstrated that two agents can be actuated independently by using time-division multiplexing signals. This means that the signal was divided into short time intervals alternating between the two Eigen frequencies of the robots. The experiments showed the stand-still of one agent while the other one is moving, as well the simultaneous movement at different speeds. Furthermore, it was shown that the direction of motion of a MagMite can change with input frequency, for example, moving backwards or sidewise, which would allow the implementation of more independent motions.[75]

Mag-μBots have a simple rectangular design and are actuated by an oscillating field to create a type of slip–stick motion on arbitrary surfaces. By using variable lengths, they respond with different speeds to an applied field. Again, the input signal is a combination of alternating inputs switching between the two microrobot prototypes. Consequently, the microrobots move towards their individual goals in a type of zigzag motion.[98] Furthermore, microrobots can be addressed selectively by using "programmable" composite magnetic materials.[99]

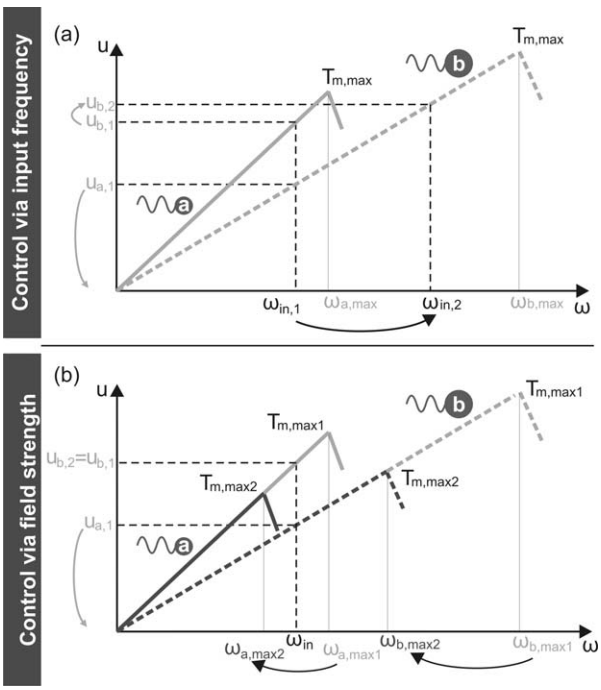

Fig. 10 Actuation inputs for selective control. The schematic shows typical frequency–velocity responses of two ABF prototypes "a" and "b" with variable slopes and step-out frequencies $\omega_{a,max}$ and $\omega_{b,max}$. ω_{in} represents the frequency of the actuation input and $T_{m,max}$ corresponds to the maximum magnetic torque, which is a function of the applied field strength. The step-out frequencies are a function of $T_{m,max}$. (a) Selective control *via* frequency input. $T_{m,max}$ is kept constant. At $\omega_{in,1}$ both ABF prototypes swim at velocities $u_{a,1}$ and $u_{b,1}$, respectively. After increasing the input frequency to $\omega_{in,2}$, only prototype 'b' can swim in-sync and prototype 'a' drops out. (b) Selective control *via* field strength. The input frequency ω_{in} is kept constant. The magnetic torque is decreased from $T_{m,max1}$ to $T_{m,max2}$, which leads to a decrease of the step-out frequency of both prototypes. The decrease of $T_{m,max}$ is chosen such that the step-out frequency of prototype 'a' $\omega_{a,max2}$ drops below the input frequency ω_{in}, while the step-out frequency $\omega_{b,max2}$ remains above it.

Frequency-dependent behavior of ABFs for individual control

Similar to the surface walkers, ABFs can also be designed to operate at different speeds at a given frequency. At a given magnetic field strength, the velocity of a helical microrobot is a function of the frequency of the applied field as given by eqn (21)

$$u = \frac{-b}{a + \Psi_v}\omega \tag{22}$$

The parameters a and b contain geometric features of the tail (see Fig. 3), and ψ_v contains the geometric features of the head. Tuning these parameters creates swimmers with different velocities, even including negative velocities if the handedness of the helix is altered. In addition, the frequency-dependent behavior of ABFs can be used for the control of individuals inside a group or swarm. The linear relationship between velocity u and the frequency ω in eqn (22) is only valid while the magnetic torque is large enough to sustain the rotation of the robot at the frequency ω. The drag on the microrobot increases with ω and the maximum frequency, referred to as *step-out frequency*, is given by the maximum magnetic torque:

$$\omega_{max} = \frac{(a + \Psi_v)}{(a + \Psi_v)(c + \Psi_\omega) - b^2} T_{m,max} \tag{23}$$

If the magnetic field is rotated at a frequency higher than ω_{max}, the robot cannot move in-sync with the field anymore and the velocity drops. This phenomenon has already been reported multiple times.[23,87,94,100] From eqn (13) it is clear that the maximum $T_{m,max}$ is a function of the applied magnetic field strength, the magnetization and the size of the magnetic material on the swimmer. The magnetic field strength is the same for all microrobots, but the magnetization and size are

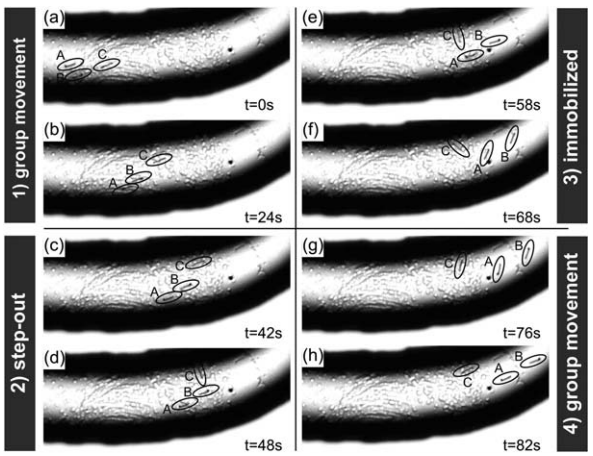

Fig. 11 Selective control of an individual ABF inside a "swarm". Two prototypes A and B have a large magnetic head, *i.e.* high step-out frequency, prototype C has a small magnetic head, *i.e.* low step-out frequency. (a and b) Input frequency below the step-out frequency: Synchronous swimming of all three prototypes. (c and d) Input frequency is increased beyond step-out frequency of prototype C, which gets destabilized. (e and f) Prototypes A and B continue while C remains immobile. (g and h) The frequency is decreased and C resumes motion with prototypes A and B.

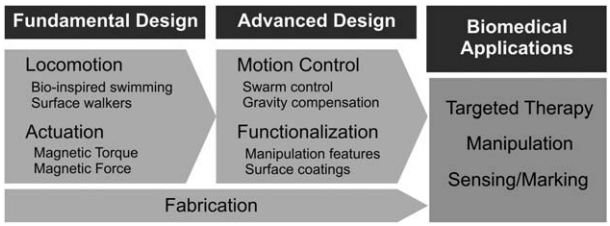

Fig. 12 Design challenges of magnetic microrobots for biomedical applications.

tunable parameters with which microrobots of variable step-out frequencies can be designed.[101]

This results in an input-frequency range at which one type of microrobot can still move in-sync with the field, while another is slowed down or brought to a stand-still because its maximum actuation frequency is overstepped. In an example where two robot designs are used, there exists a region in the actuation input range where both microrobots follow the field, and another region exists where only the design with the higher step-out frequency follows the input. There are two approaches to switch between these two regions. One way is to change the frequency of the applied field, the other is to change the magnetic field strength, and therefore $T_{m,max}$, which decreases ω_{max} (see Fig. 10).

Fig. 11 shows experimental results of decoupling an individual ABF from a group of three. Two prototypes, labeled A and B, have large magnetic heads, *i.e.* a large ω_{max}, and prototype *C* has a small magnetic head with a small step-out frequency. They are moved simultaneously during the first 42 seconds (Fig. 11a and b), then the input frequency is increased beyond ω_{max} of prototype *C* (Fig. 11c and d). This results in a de-stabilization and subsequent stand-still of prototype C, while A and B continue swimming (Fig. 11e and f). By decreasing the frequency once more, prototype C is re-activated and synchronous swimming of the whole group is resumed (Fig. 11g and h).

Another type of behavior observed in ABFs is the frequency-dependent precession and associated variance in the drift velocity. Many surface walkers that use a rotating magnetic field rely on the drag-imbalance near a surface to create their propulsion. This drag imbalance results in a sidewise drift in the case of helical microrobots moving near a surface. It was previously reported that the frequency-dependent precession, or tumbling, changes the drift propulsion, effectively leading to a variable sidewise motion for different input frequencies.[94] As mentioned with the MagMites above, this additional feature could lead to a more complex motion control of ABFs.

Summary and outlook

Microrobots are promising tools for biomedical applications, such as targeted drug delivery or cell manipulation. The fundamental challenges are to find suitable locomotion and actuation methods for microrobots (see Fig. 12). Magnetic actuation is suitable for *in vitro* as well as *in vivo* applications as the required field-strengths are harmless to humans and microorganisms. It has been shown that various robot designs can be actuated with magnetic fields. Some are driven by a magnetic force, some by a magnetic torque. It would seem that torque-driven propulsion scales favorably over force-driven propulsion as the robot's size decreases to the micro- and nanometer scale. Hence, helical microrobots actuated by rotating magnetic fields are promising tools for microscale biomedical applications.[102]

In future, research efforts are expected to shift from fundamental design challenges to advanced microrobot design questions focusing on the integration of mechanisms and tools for specific applications. Initial results have already been achieved, for example, by adding a transport claw to a helical microrobot[25] or by developing smart surfaces that enhance the loading and controlled release of medication.[103] Swarm control will further improve the delivery capabilities of microrobots. Magnetic microrobots are expected to remain one of the most promising micro-tools for *in vivo* applications.

Acknowledgements

This work was funded by the NCCR Robotics and the European Research Council Advanced Grant BOTMED.

References

1 R. Pfeifer, M. Lungarella and F. Iida, *Science*, 2007, **318**, 1088–1093.
2 B. J. Nelson, I. K. Kaliakatsos and J. J. Abbott, *Annu. Rev. Biomed. Eng.*, 2010, **12**, 55–85.
3 L. Zhang, K. E. Peyer and B. J. Nelson, *Lab Chip*, 2010, **10**, 2203–2215.
4 J. J. Abbott, K. E. Peyer, M. C. Lagomarsino, L. Zhang, L. Dong, I. K. Kaliakatsos and B. J. Nelson, *Int. J. Rob. Res.*, 2009, **28**, 1434–1447.
5 P. Fischer and A. Ghosh, *Nanoscale*, 2011, **3**, 557–563.
6 E. M. Purcell, *Am. J. Phys.*, 1977, **45**, 3–11.
7 E. Lauga, *Phys. Fluids*, 2007, **19**, 1–21.
8 E. Lauga and D. Bartolo, *Phys. Rev. E: Stat., Nonlinear, Soft Matter Phys.*, 2008, **78**, 030901.
9 P. Metzner, *Arch. Gesch. Math., Naturwiss. Tech.*, 1923, 365–372.
10 R. N. Doetsch, *J. Theor. Biol.*, 1966, **11**, 411–417.
11 H. C. Berg and R. Anderson, *Nature*, 1973, **245**, 380–382.
12 K. E. Schreiner, *J. Biomech.*, 1971, **4**, 73–83.
13 S. Guo, J. Sawamoto, and Q. Pan, *IEEE Int. Conf. Intelligent Robots Systems*, 2005, pp. 1047–1052.
14 S. Guo, Q. Pan and M. B. Khamesee, *Microsyst. Technol.*, 2007, **14**, 307–314.
15 R. Dreyfus, J. Baudry, M. L. Roper, M. Fermigier, H. A. Stone and J. Bibette, *Nature*, 2005, **437**, 862–865.
16 S. Melle, O. Calderón, M. Rubio and G. Fuller, *Phys. Rev. E: Stat. Phys., Plasmas, Fluids, Relat. Interdiscip. Top.*, 2003, **68**, 041503.
17 M. Roper, R. Dreyfus, J. Baudry, M. Fermigier, J. Bibette and H. A. Stone, *J. Fluid Mech.*, 2006, **554**, 167–190.
18 M. Roper, R. Dreyfus, J. Baudry, M. Fermigier, J. Bibette and H. A. Stone, *Proc. R. Soc. London, Ser. A*, 2008, **464**, 877–904.

19 J. J. Benkoski, R. M. Deacon, H. B. Land, L. M. Baird, J. L. Breidenich, R. Srinivasan, G. V. Clatterbaugh, P. Y. Keng and J. Pyun, *Soft Matter*, 2010, **6**, 602–609.
20 J. J. Benkoski, J. L. Breidenich, O. M. Uy, A. T. Hayes, R. M. Deacon, H. B. Land, J. M. Spicer, P. Y. Keng and J. Pyun, *J. Mater. Chem.*, 2011, **21**, 7314–7325.
21 D. J. Bell, S. Leutenegger, K. M. Hammar, L. X. Dong and B. J. Nelson, *IEEE Int. Conf. Robot. Autom.*, 2007, 1128–1133.
22 L. Zhang, J. J. Abbott, L. Dong, B. E. Kratochvil, D. Bell and B. J. Nelson, *Appl. Phys. Lett.*, 2009, **94**, 064107.
23 L. Zhang, J. J. Abbott, L. Dong, K. E. Peyer, B. E. Kratochvil, H. Zhang, C. Bergeles and B. J. Nelson, *Nano Lett.*, 2009, **9**, 3663–3667.
24 A. Ghosh and P. Fischer, *Nano Lett.*, 2009, **9**, 2243–2245.
25 S. Tottori, L. Zhang, F. Qiu, K. K. Krawczyk, A. Franco-Obregón and B. J. Nelson, *Adv. Mater.*, 2012, **24**, 811–816.
26 W. Ludwig, *J. Comp. Physiol. A -Neuroethol. Sens. Neural Behav. Physiol.*, 1930, **13**, 397–504.
27 A. Shah and Y. Ben-Shahar, *Science*, 2009, **325**, 1131–1134.
28 T. Sanchez, D. Welch, D. Nicastro and Z. Dogic, *Science*, 2011, **333**, 456–9.
29 B. Evans, A. R. Shields, R. L. Carroll, S. Washburn, M. R. Falvo and R. Superfine, *Nano Lett.*, 2007, **7**, 1428–1434.
30 E. M. Gauger, M. T. Downton and H. Stark, *Eur. Phys. J. E*, 2009, **28**, 231–242.
31 F. Fahrni, M. W. J. Prins and L. J. van Ijzendoorn, *Lab Chip*, 2009, **9**, 3413–3421.
32 J. Belardi, N. Schorr, O. Prucker and J. Rühe, *Adv. Funct. Mater.*, 2011, **21**, 3314–3320.
33 S. N. Khaderi, C. B. Craus, J. Hussong, N. Schorr, J. Belardi, J. Westerweel, O. Prucker, J. Rühe, J. M. J. den Toonder and P. R. Onck, *Lab Chip*, 2011, **11**, 2002–2010.
34 J. Hussong, N. Schorr, J. Belardi, O. Prucker, J. Rühe and J. Westerweel, *Lab Chip*, 2011, **11**, 2017–2022.
35 M. Vilfan, A. Potocnik, B. Kavcic, N. Osterman, I. Poberaj, A. Vilfan and D. Babic, *Proc. Natl. Acad. Sci. U. S. A.*, 2010, **107**, 1844–1847.
36 A. Babataheri, M. Roper, M. Fermigier and O. Du Roure, *J. Fluid Mech.*, 2011, **678**, 5–13.
37 N. Coq, A. Bricard, F.-D. Delapierre, L. Malaquin, O. du Roure, M. Fermigier and D. Bartolo, *Phys. Rev. Lett.*, 2011, **107**, 014501.
38 J. L. Breidenich, M. C. Wei, G. V. Clatterbaugh, J. J. Benkoski, P. Y. Keg and J. Pyun, *Soft Matter*, 2012, **8**, 5334–5341.
39 G. J. Hancock, *Proc. R. Soc. London, Ser. A*, 1953, **217**, 96–121.
40 J. Gray and G. Hancock, *J. Exp. Biol.*, 1955, **32**, 802–814.
41 R. G. Cox, *J. Fluid Mech.*, 1970, **44**, 791–810.
42 J. Lighthill, *SIAM Rev.*, 1976, **18**, 161–230.
43 C. Brennen and H. Winet, *Annu. Rev. Fluid Mech.*, 1977, **9**, 339–398.
44 J. J. L. Higdon, *J. Fluid Mech.*, 1979, **94**, 331–351.
45 J. Lighthill, *J. Eng. Math.*, 1996, **30**, 35–78.
46 E. Lauga and T. R. Powers, *Rep. Prog. Phys.*, 2009, **72**, 096601.
47 B. Behkam and M. Sitti, *ASME Int. Mech. Eng. Congr. Expo., 2005*, 2004, 1037–1041.
48 R. E. Johnson and C. J. Brokaw, *Biophys. J.*, 1979, **25**, 113–127.
49 A. W. Mahoney, J. C. Sarrazin, E. Bamberg and J. J. Abbott, *Adv. Rob.*, 2011, **25**, 1007–1028.
50 E. Lauga, W. R. DiLuzio, G. M. Whitesides and H. A. Stone, *Biophys. J.*, 2006, **90**, 400–412.
51 A. Itoh, *IEEE/ASME Trans. Mechatron.*, 2000, **5**, 181–188.
52 B. Behkam and M. Sitti, *Proc. IEEE EMBS Ann. Int. Conf.*, 2006, 2421–2424.
53 B. Behkam and M. Sitti, *Proc. IEEE RAS-EMBS Int. Conf. Biomedical Robotics and Biomechatronics*, 2008, pp. 753–757.
54 H. Bae, S. Park, J. Kim, B. Lim, J. Park and S. Park, *IEEE International Conference on Robotics and Biomimetics*, 2009, pp. 7–12.
55 S. Martel, M. Mohammadi, O. Felfoul, Z. Lu and P. Pouponneau, *Int. J. Rob. Res.*, 2009, **28**, 571–582.
56 S. Martel and M. Mohammadi, in *Proc. IEEE International Conference on Robotics and Actuation*, IEEE, 2010, pp. 500–5.
57 S. Sánchez and M. Pumera, *Chem.–Asian J.*, 2009, **4**, 1402–1410.
58 S. Sanchez, A. A. Solovev, S. Schulze and O. G. Schmidt, *Chem. Commun.*, 2011, **47**, 698–700.
59 W. Gao, S. Sattayasamitsathit, K. M. Manesh, D. Weihs and J. Wang, *J. Am. Chem. Soc.*, 2010, **132**, 14403–14405.
60 G.-L. Jiang, Y.-H. Guu, C.-N. Lu, P.-K. Li, H.-M. Shen, L.-S. Lee, J. A. Yeh and M. T.-K. Hou, *J. Micromech. Microeng.*, 2010, **20**, 085042.
61 A. W. Mahoney and J. J. Abbott, *Appl. Phys. Lett.*, 2011, **99**, 134103.
62 H. Morimoto, T. Ukai, Y. Nagaoka, N. Grobert and T. Maekawa, *Phys. Rev. E: Stat., Nonlinear, Soft Matter Phys.*, 2008, **78**, 021403.
63 C. E. Sing, L. Schmid, M. F. Schneider, T. Franke and A. Alexander-Katz, *Proc. Natl. Acad. Sci. U. S. A.*, 2010, **107**, 535–540.
64 M. Karle, J. Wöhrle, J. Miwa, N. Paust, G. Roth, R. Zengerle and F. Stetten, *Microfluid. Nanofluid.*, 2010, **10**, 935–939.
65 M. T. Hou, H.-M. Shen, G.-L. Jiang, C.-N. Lu, I.-J. Hsu and J. A. Yeh, *Appl. Phys. Lett.*, 2010, **96**, 024102.
66 L. O. Mair, B. Evans, A. R. Hall, J. Carpenter, A. Shields, K. Ford, M. Millard and R. Superfine, *J. Phys. D: Appl. Phys.*, 2011, **44**, 125001.
67 L. Zhang, Y. Lu, L. Dong, R. Pei, J. Lou, B. E. Kratochvil and B. J. Nelson, *Proc. IEEE Nano*, 2009, **8**, 487–490.
68 L. Zhang, T. Petit, Y. Lu, B. E. Kratochvil, K. E. Peyer, R. Pei, J. Lou and B. J. Nelson, *ACS Nano*, 2010, **4**, 6228–6234.
69 T. Petit, L. Zhang, K. E. Peyer, B. E. Kratochvil and B. J. Nelson, *Nano Lett.*, 2012, **12**, 156–160.
70 E. J. Smith, D. Makarov, S. Sanchez, V. M. Fomin and O. G. Schmidt, *Phys. Rev. Lett.*, 2011, **107**, 097204.
71 V. M. Fomin, E. J. Smith, D. Makarov, S. Sanchez and O. G. Schmidt, *Phys. Rev. B: Condens. Matter Mater. Phys.*, 2011, **84**, 174303.
72 C. Pawashe, S. Floyd and M. Sitti, *Int. J. Rob. Res.*, 2009, **28**, 1077–1094.

73 E. Diller, S. Floyd, C. Pawashe and M. Sitti, *IEEE Trans. Rob.*, 2012, **28**, 172–182.
74 K. Vollmers, D. R. Frutiger, B. E. Kratochvil and B. J. Nelson, *Appl. Phys. Lett.*, 2008, **92**, 144103.
75 D. R. Frutiger, K. Vollmers, B. E. Kratochvil and B. J. Nelson, *Int. J. Rob. Res.*, 2009, **29**, 613–636.
76 H.-W. Tung, D. R. Frutiger, S. Pané and B. J. Nelson, *IEEE Int. Conf. Robot. Autom.*, 2012, 715–720.
77 Z. Nagy, D. R. Frutiger, R. I. Leine, C. Glocker and B. J. Nelson, *IEEE Int. Conf. Rob. Autom.*, 2010, 1598–1603.
78 E. B. Steager, M. S. Sakar, C. Magee, M. Kennedy, A. Cowley and V. Kumar, *IEEE Int. Conf. Robot. Autom.*, 2012, 3541–3542.
79 B. E. Kratochvil, M. P. Kummer, S. Erni, R. Borer, D. R. Frutiger, S. Schuerle and B. J. Nelson, *Proceedings International Symposium on Experimental Robotics*, 2010, pp. 1–13.
80 S. Schürle, K. E. Peyer, B. E. Kratochvil and B. J. Nelson, *IEEE Int. Conf. Robot. Autom.*, 2012, 1081–1086.
81 O. Pironneau, *J. Fluid Mech.*, 1973, **59**, 117–128.
82 J.-M. Bourot, *J. Fluid Mech.*, 1974, **65**, 513–515.
83 J. J. Abbott, O. Ergeneman, M. P. Kummer, A. M. Hirt and B. J. Nelson, *IEEE Trans. Rob.*, 2007, **23**, 1247–1252.
84 M. P. Kummer, J. J. Abbott, B. E. Kratochvil, R. Borer, A. Sengul and B. J. Nelson, *IEEE Trans. Rob.*, 2010, **26**, 1006–1017.
85 C. Bergeles, B. E. Kratochvil and B. J. Nelson, *IEEE Trans. Rob.*, 2012, **28**, 798–809.
86 P. Vartholomeos, M. Fruchard, A. Ferreira and C. Mavroidis, *Annu. Rev. Biomed. Eng.*, 2011, **13**, 157–184.
87 T. W. R. Fountain, P. V. Kailat and J. J. Abbott, in *Proc. IEEE International Conference on Robotics and Actuation*, IEEE, 2010, pp. 576–581.
88 A. W. Mahoney, D. L. Cowan, K. M. Miller and J. J. Abbott, *IEEE Int. Conf. Robot. Autom.*, 2012, 3375–3380.
89 A. W. Mahoney, N. D. Nelson, E. M. Parsons and J. J. Abbott, *IEEE Int. Conf. Intelligent Robots Systems*, 2012, 3559–3564.
90 K. E. Peyer, S. Tottori, F. Qiu, L. Zhang and B. J. Nelson, *Chem.–Eur. J.*, 2012, DOI: 10.1002/chem.20123364.
91 S. Schuerle, S. Pané, E. Pellicer, J. Sort, M. D. Baró and B. J. Nelson, *Small*, 2012, **8**, 1498–1502.
92 F. Qiu, L. Zhang, S. Tottori and B. J. Nelson, *Microelectron. Eng.*, 2012, submitted.
93 K. Kobayashi and K. Ikuta, *Appl. Phys. Lett.*, 2008, **92**, 262505.
94 K. E. Peyer, L. Zhang, B. E. Kratochvil and B. J. Nelson, in *Proceedings IEEE International Conference on Robotics and Actuation*, 2010, pp. 96–101.
95 M. Sendoh, K. Ishiyama, K. I. Arai, M. Jojo, F. Sato and H. Matsuki, *IEEE Trans. Magn.*, 2002, **38**, 3359–3361.
96 K. E. Peyer, L. Zhang and B. J. Nelson, *Appl. Phys. Lett.*, 2011, **99**, 174101.
97 E. Diller, Z. Ye and M. Sitti, in *IEEE International Conference Intelligent Robots Systems*, San Francisco, CA, USA, 2011, pp. 1291–1296.
98 E. Diller, S. Floyd, C. Pawashe and M. Sitti, *IEEE Trans. Rob.*, 2012, **28**, 172–182.
99 E. Diller, S. Miyashita and M. Sitti, *IEEE Int. Conf. Robots and Intelligent Systems*, 2012, 2325–2331.
100 K. Ishiyama, M. Sendoh, A. Yamazaki, M. Inoue and K. I. Arai, *IEEE Trans. Magn.*, 2001, **37**, 2868–2870.
101 M. Sendoh, K. Ishiyama and K. I. Arai, *IEEE Trans. Magn.*, 2002, **38**, 3356–3358.
102 F. Qiu, L. Zhang, S. Tottori, K. Marquardt, K. Krawczyk, A. Franco-Obregon and B. J. Nelson, *Mater. Today*, 2012, **10**, 463.
103 J. Pokki, O. Ergeneman, K. M. Sivaraman, B. Ozkale, M. a. Zeeshan, T. Lühmann, B. J. Nelson and S. Pané, *Nanoscale*, 2012, **4**, 3083–3088.
104 S. Floyd, C. Pawashe and M. Sitti, *IEEE Int. Conf. Robot. Autom.*, 2008, 419–424.

